

BOND AND ANCHORAGE LENGTH OF NEAR-SURFACE MOUNTED FRP RODS IN CONCRETE

Laura De Lorenzis, University of Lecce, Lecce, ITALY

Andrea Rizzo, University of Lecce, Lecce, ITALY

Antonio La Tegola, University of Lecce, Lecce, ITALY

Abstract

Near-surface mounted (NSM) Fiber Reinforced Polymer (FRP) rods are being increasingly used as alternative to externally bonded FRP laminates for enhancing flexural and shear strength of deficient reinforced concrete, prestressed concrete, masonry and timber members. In order for this strengthening technique to perform effectively, bond between the NSM reinforcement and the substrate material is a critical issue. Following up to previous investigations, a different type of specimen was designed in order to obtain a test procedure as efficient and reliable as possible. Such procedure was then used to investigate the effect of some significant variables on the bond performance, and to confirm and more precisely quantify the trends indicated by previous experimental data. Obtainment of the local bond stress-slip relationship of NSM FRP rods allows computation of the anchorage length required in design.

Introduction and Objective

A new strengthening technique based on fiber-reinforced polymer (FRP) composites has been recently emerging as a valid alternative to externally bonded FRP laminates. It is based on the use of FRP rods as superficial shear or flexural reinforcement and will be referred to as near-surface mounted (NSM) FRP rods.

This technique has been defined as “*the new millennium’s version of rebar slotting or ‘stitching dogs’*” [1]. In fact, although the use of FRP rods for this application is very recent, NSM steel rods have been used in Europe for strengthening of RC structures since the early 50's [2]. The advantages of FRP versus steel for this application are primarily the better resistance to corrosion, the ease and speed of application due to the lightweight properties, and the optimization of the grooving process. Due to the high tensile strength of the FRP, rods with smaller diameters can be used for a given required tensile force, which reduces the groove size needed for embedment. Further reduction in depth is due to the better corrosion resistance and possibly to the better bond behavior of ribbed FRP rods with respect to steel rebars. When splitting of the groove-filling material controls bond failure, it is very likely that, for a given cover, rebars with stiffer surface deformations like steel have a greater tendency to induce splitting than FRP rods, the latter having soft surface deformations made of polymer resin.

The use of NSM FRP rods is an attractive method for increasing flexural and shear strength of deficient reinforced concrete members and masonry walls and, in certain cases, can be more convenient than using FRP laminates. Application of NSM FRP rods does not require surface preparation work (other than grooving) and implies minimal installation time compared to FRP laminates. The use of customized grooving tools can allow technicians to cut the appropriate grooves in one pass, whereas the choice of high-viscosity epoxies as groove-filling material allows to easily gun the material in the groove even when strengthening members for positive moments. Another advantage is the feasibility of anchoring these rods into members adjacent to the one to be strengthened. Furthermore, this technique becomes particularly attractive for strengthening in the negative moment regions of slabs and decks, where external reinforcement would be subjected to mechanical and environmental damage and would require protective cover which could interfere

with the presence of floor finishes. Finally, NSM rods offer better fire performance compared to externally bonded laminates, due to protection of the encapsulating material.

The literature currently available on NSM FRP rods is relatively limited. Beside field applications and experimental field projects, laboratory projects on NSM FRP rods for structural strengthening of concrete members have been mainly carried out during the past three years [3-8].

In order for the NSM-rods strengthening technique to perform effectively, bond between the NSM reinforcement and the substrate material is a critical issue. Bond of NSM rods embedded in concrete has been investigated thus far in a few different test series [4,5,8], all involving different test methods. This test program follows up to a previous investigation [9], in which a new specimen was designed to reduce the limitations encountered in the previous bond test series on NSM FRP rods. Aim of this work was to use such specimen configuration to enlarge the experimental database on bond of NSM FRP rods and clarify the influence on the bond performance of variables such as the surface preparation of the groove, the rod surface configuration and the groove depth.

Experimental Tests

Test Specimen

The specimen used for this investigation is shown in Figure 1. It consists of a C-shaped concrete block with a square groove in the middle for embedment of the NSM rod. The dimensions of the block were designed, upon a preliminary phase of testing, to ensure that no transverse cracking would occur in the specimen before bond failure of the NSM rod and that, in case of bond failure by concrete cracking, the crack pattern would not be influenced by the specimen width. Dimension s_p in Figure 1 depends on the groove size and is such that the FRP rod, once applied, is situated in the middle of the specimen cross-section. The distance u is such that no fastening-type failure occurs in the concrete above the bonded length. The applied load is reacted by means of four steel threaded rods at the four corners of the block inserted into a stiffened steel plate.

This specimen offers the advantages of the direct pull-out type of test (manageable specimen size, possibility to conduct the test in slip-control mode and to measure both loaded-end and free-end slip, visual access to the test zone during loading). At the same time, it does not need to use two or even four bonded lengths of FRP rod for reaction and thus minimizes the problem of eccentricity, the preparation time and the use of material.

Test Variables, Materials, and Procedure

The specimens tested in this phase of the project are illustrated in Table 1. The test variables were: bonded length (equal to 4 and 24 times the *nominal* rod diameter), groove size (equal to approximately 1.3, 1.6, and 2.2 times the *actual* rod diameter), and rod type (Carbon FRP, CFRP, ribbed and Glass FRP, GFRP, ribbed). As part of a previous experimental study [9], specimens with 4-diameter bonded length and same values of the remaining parameters had been tested. The only difference was that, in that study, the grooves in which the rods were embedded had been pre-formed rather than saw-cut, and therefore had a smooth surface. As a result, in most specimens the joint had failed at the epoxy-concrete interface. Testing the same specimens with saw-cut grooves would allow to evaluate the influence of the groove surface preparation on the bond performance. It could be noted that, when repairing/strengthening a concrete member, it is often required that the geometry of the member be reconstructed with the addition of new concrete, therefore, the grooves might be pre-formed rather than cut even in a real situation.

Apart from the different material properties, CFRP and GFRP ribbed rebars (Figure 2) differed for the height of the surface deformations (ribs), more pronounced for the GFRP rods than for the CFRP ones. Using the traditional terminology of steel rebars, it could be said that the GFRP rebars had a higher relative rib area than the CFRP ones. For the purpose of computing the bonded length as a multiple of the diameter, the nominal diameter was used, which is the dimension of interest in the design process. However, for the purpose of computing the groove size as a multiple of

the diameter, the actual dimensions of the rod rather than the nominal ones are significant. The groove-size-to-actual-bar-diameter ratio has been termed k and reported in Table 1. Such parameter (related to the cover-thickness-to-bar-diameter ratio) is expected to have similar significance to the cover-thickness-to-bar-diameter ratio in the context of bond of internal reinforcement in concrete [10]. For the ribbed rods, a conventional diameter was computed as the average between the maximum and minimum diameters obtained by including and excluding the rib height on both sides of the core. The nominal rod diameter was used in computation of the bond stress and strength at the interface between rod and epoxy.

Prior to starting the bond test series, a detailed material characterization was carried out. The concrete had an average compressive strength of 22 MPa and a tensile strength (calculated as 90% of the experimental splitting strength according to the CEB-FIP MC90 [11]) of 2.2 MPa. The maximum size of aggregate was 15 mm. The epoxy paste had a direct tensile strength of 28 MPa. The ribbed GFRP rods had 9.5-mm nominal diameter, 873-MPa tensile strength and 37.17-GPa Young's modulus, and the ribbed CFRP rods had 9.5-mm nominal diameter, 2014-MPa tensile strength and 109.27-GPa Young's modulus.

The specimen was instrumented with two LVDTs, to monitor slip of the NSM bar with respect to the concrete at both the loaded end and the free end of the bonded length (Figure 1). Testing was conducted in displacement-control mode on a 200-kN universal testing machine with a 0.2 mm/min cross-head displacement rate.

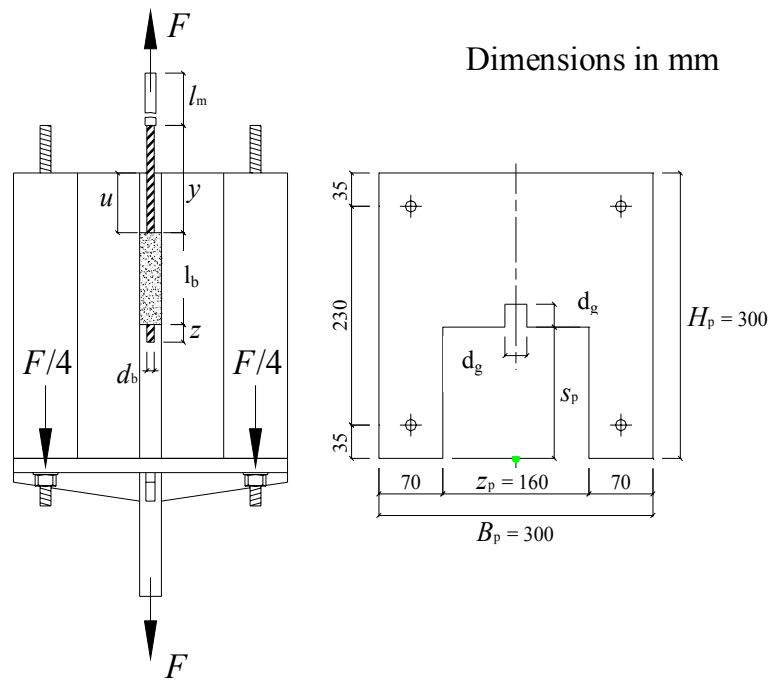


Figure 1. Test Specimen

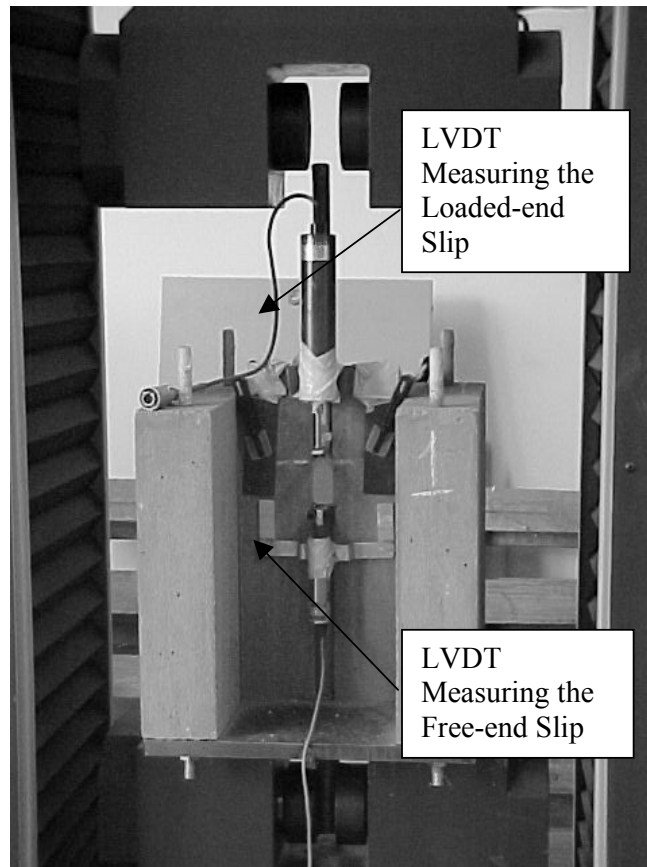
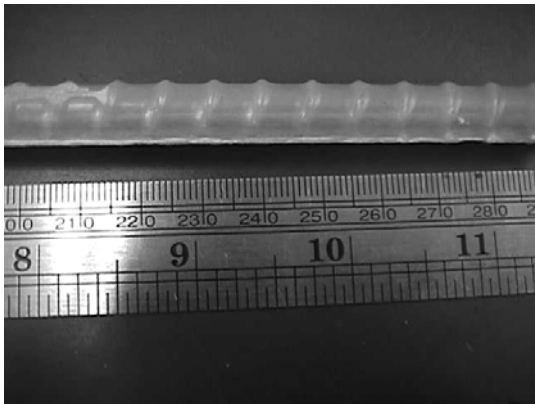
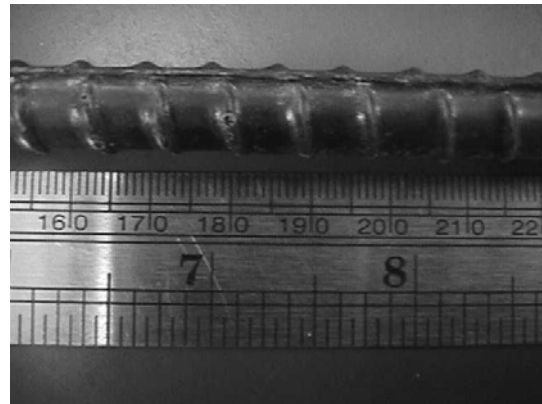


Figure 1 (cont'd). Test Specimen



(a)



(b)

Figure 2. Ribbed GFRP (a) and CFRP (b) Rods

Table 1. Test Program

Specimen Code	Rod Type	d_g (mm)	Actual d_b (mm)	k	l_a (n° of nominal d_b)
CR/104/a	Ribbed/CFRP	15	11.3	1.33	4
CR/104/b	Ribbed/CFRP	18	11.3	1.59	4
CR/104/c	Ribbed/CFRP	24	11.3	2.12	4
CR/124/a	Ribbed/CFRP	14	11.3	1.24	24
CR/124/b	Ribbed/CFRP	18	11.3	1.59	24
CR/124/c	Ribbed/CFRP	24	11.3	2.12	24
GR/104/a	Ribbed/GFRP	15	11.0	1.36	4
GR/104/b	Ribbed/GFRP	18	11.0	1.64	4
GR/104/c	Ribbed/GFRP	24	11.0	2.18	4
GR/124/a	Ribbed/GFRP	14	11.0	1.27	24
GR/124/b	Ribbed/GFRP	18	11.0	1.64	24
GR/124/c	Ribbed/GFRP	24	11.0	2.18	24

Test Results

Specimen Behavior and Failure Mode

The main test results are reported in Table 2. Failure occurred for all specimens by cracking of the concrete surrounding the groove accompanied by formation of splitting cracks in the epoxy cover (Figure 3). The sequence of stages observed in behavior of all specimens is as follows: (a) at low load levels (typically up to about 50% of the ultimate load), no cracks are visible on epoxy and concrete; (b) for a load close to about 50% of the ultimate load, a typical crackling noise reveals the onset of internal microcracking in the epoxy; (c) soon after beginning of the noise, a longitudinal splitting crack starts in the epoxy cover at the rod loaded end, but no cracking is yet visible in the concrete surrounding the groove; (d) the crack propagates longitudinally in the epoxy towards the rod free end; at the same time, aside the portion of bonded length where the epoxy cover is already cracked, the profile of a superficial crack starts appearing in the concrete. This indicates that cracking of the epoxy relieves the circumferential stresses in the bar cover which balance the radial components of the bond stresses. Such components must then be balanced by tensile stresses in the concrete which soon exceed the concrete tensile strength and lead to the formation of cracks along inclined planes; (e) the concrete crack extends along the entire bonded length and opens up, until the concrete delimited by the crack along with the epoxy cover is finally expelled.

Some differences could be observed between specimens with CFRP and GFRP rods. In the first ones, the maximum load was reached after propagation of the epoxy longitudinal crack and formation of the concrete crack. At this point, the load started decreasing as the concrete crack width increased, as the faces separated by the crack still had some cohesive strength left due to aggregate interlocking. Qualitatively, the average bond stress vs. slip curves of specimens CR/104 (Figure 4-a) are similar to the curves giving the concrete tensile stress across a crack vs. the crack opening displacement (see for example [12] or [13]). This makes sense, as the average bond stress τ (which can be approximately regarded as the local bond stress for short bonded lengths) can be considered proportional to the radial pressure p exerted by the rod on the surrounding cover:

$$\tau = p \cdot \tan \gamma \quad (1)$$

which in turn is reacted, in the final stage, by tensile stresses in the concrete; and the longitudinal slip is accompanied by gradual opening of the crack (Figure 3-c). In equation (1), $\tan \gamma$ is the coefficient of friction and cohesion is neglected. Conversely, in specimens with GFRP rods, the higher relative

rib area led to a more explosive failure, and the bond stress – slip curves were as shown in Figure 4-b.

Table 2. Test Results

Spec. Code	P_{max} [kN]	$\frac{P_{max}}{P_u} \cdot 100$ [%]	τ_{avu} [MPa]	$(s_{le})_{lim}$ [mm]	$(s_{fe})_{lim}$ [mm]	Failure Mode
CR/104/a	13.12	9.2	11.24	0.304	0.102	Splitting + Concr. Cracking
CR/104/b	17.91	12.5	15.35	0.287	0.034	Splitting + Concr. Cracking
CR/104/c	19.33	13.5	16.56	1.549	0.206	Splitting + Concr. Cracking
CR/124/a	52.16	36.5	7.45	2.128	0.372	Splitting + Concr. Cracking
CR/124/b	50.80	35.6	7.25	0.454	0.152	Splitting + Concr. Cracking
CR/124/c	66.47	46.6	9.49	0.560	0.198	Splitting + Concr. Cracking
GR/104/a	10.67	17.2	9.14	0.125	0.024	Splitting + Concr. Cracking
GR/104/b	14.68	23.7	12.58	N/A	N/A	Splitting + Concr. Cracking
GR/104/c	14.57	23.5	12.48	1.224	0.130	Splitting + Concr. Cracking
GR/124/a	26.45	42.7	3.78	1.457	0.016	Splitting + Concr. Cracking
GR/124/b	39.55	63.9	5.65	1.864	0.000	Splitting + Concr. Cracking
GR/124/c	32.04	51.8	4.58	1.310	0.068	Splitting + Concr. Cracking

P_{max} = Ultimate (peak) load of the specimen; P_u = Ultimate tensile load of the FRP rod;

τ_{avu} = Average bond stress at failure; $(s_{le})_{lim}$ = Loaded-end slip corresponding to the peak load; $(s_{fe})_{lim}$ = Free-end slip corresponding to the peak load; N/A = Not available

Effect of bonded length and groove size

For a given depth of the groove, the ultimate load of the joint increases as the bonded length increases. However, the average bond strength decreases, due to the non-uniform distribution of the bond stresses along the bonded length.

For a given bonded length, the ultimate load and the average bond strength, τ_{avu} :

$$\tau_{avu} = \frac{P_{max}}{\pi \cdot d_b l_b} \quad (2)$$

increase for increasing groove size, as the bigger cover depth delays the occurrence of splitting and cracking phenomena.

Effect of Rod Surface Configuration

As observed previously, failure of specimens with short bonded length was more explosive for GFRP than for CFRP rebars, due to the more pronounced deformations on the surface of the first ones. From Table 2 it is also evident that the bond failure load (or, equivalently, the average bond strength) of specimens with GFRP rebars was always lower than that of specimens with CFRP rebars and the same values of the remaining parameters. The reason is the higher relative rib area of GFRP, which produces a lower value of $\tan \gamma$ and thus a larger radial pressure for a given bond stress. It could be concluded that the superficial pattern of FRP rods to be used as NSM reinforcement, while being sufficiently rough to avoid failure by pull-out at the rod-epoxy interface (previous tests showed that light sandblasting is not always enough for this purpose [8]), should generate radial stresses as low as possible to delay splitting and cracking phenomena and to allow a pseudo-ductile bond – slip behavior. Further tests are underway with sanded spirally wound CFRP rods.

Effect of the Groove Surface Condition

The ultimate load of specimens CR/104/a-c and GR/104/c can be compared with that of identical specimens having smooth groove surface and failed at the epoxy – concrete interface (see [9]). As expected, the specimens with rough grooves failed in all cases at higher load levels.

However, the bond – slip relationship is also different in the two cases, and this leads to a different trend of the bond failure load as a function of the bonded length. This will be explained later.

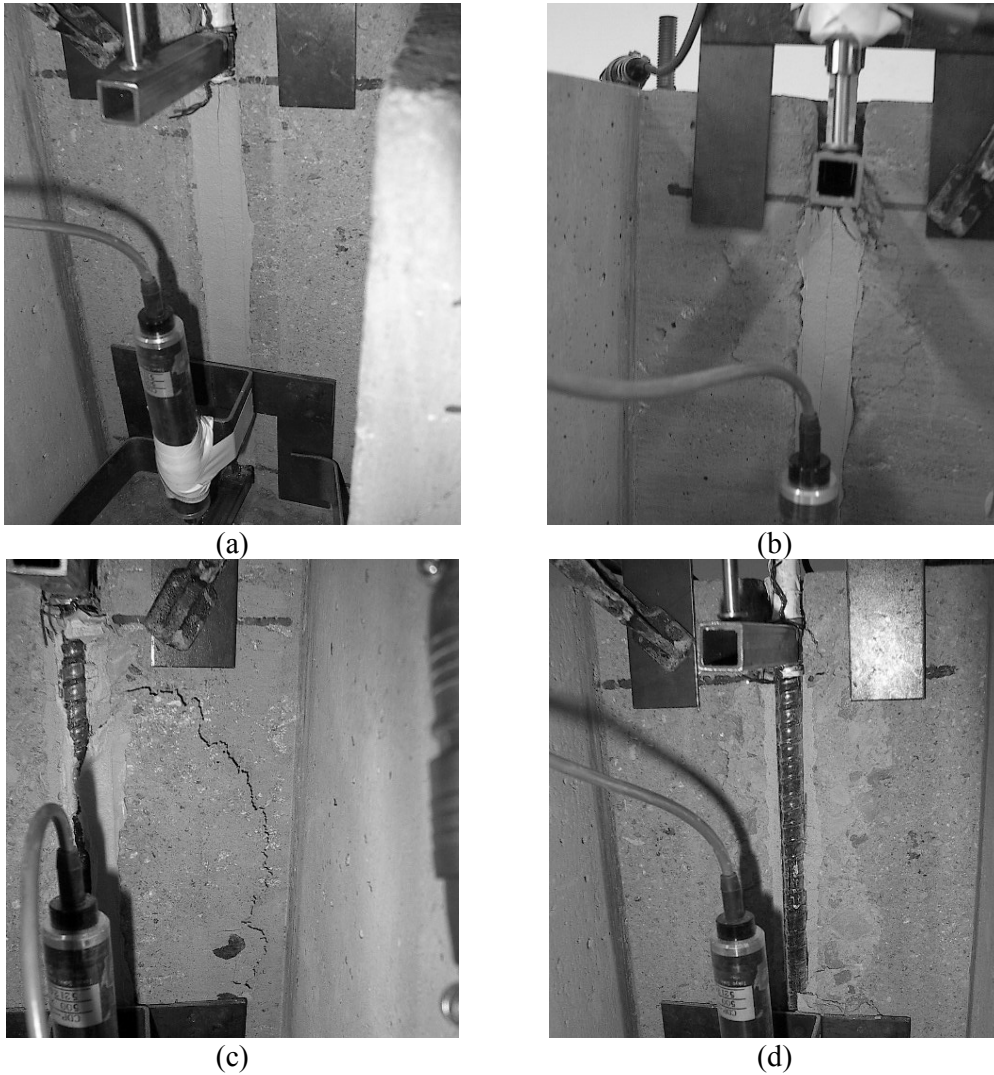
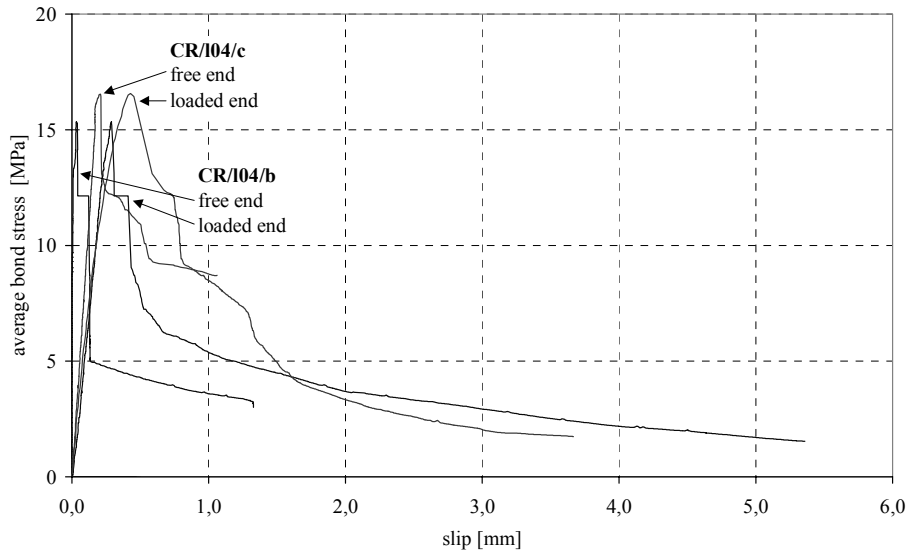
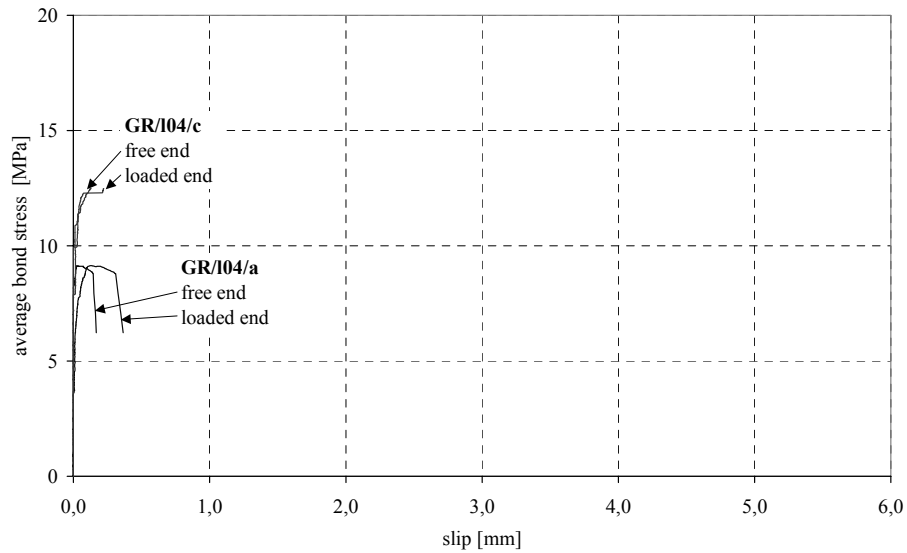


Figure 3. Typical Damage and Failure Stages of the Specimens: Formation of a Longitudinal Splitting Crack in the Epoxy Cover at the Rod Loaded End (a); Formation of Inclined Cracks in the Concrete Surrounding the Groove (b); Opening of the Concrete Cracks (c); Specimen after Failure (d).



(a)



(b)

Figure 4. Average Bond Stress vs. Slip Curves of Short Bonded Length Specimens with CFRP (a) and GFRP (b) NSM Rods

Modeling of Results

Local Bond Stress – Slip Relationship

The local bond stress – slip relationship of reinforcement in concrete is commonly approximated by the average bond stress vs. slip relationship of specimens with short bonded lengths (3 to 5 bar diameters). Hence, from the specimens with 4-diameter bonded length, the local bond stress-slip relationships can be analytically modeled. Other possibilities to obtain a local bond – slip relationship from test data are by means of load-slip curves of specimens with long bonded lengths as suggested in [14] or by means of strain data as shown in [8].

When failure is by splitting and/or concrete cracking, the bond-slip law is well interpreted by the ascending branch of the Bertero-Popov-Eligehausen (BPE) relationship, commonly used for bond of steel reinforcement in concrete [15]:

$$\tau(s) = \tau_m \cdot \left(\frac{s}{s_m} \right)^\alpha = C \cdot s^\alpha \quad 0 \leq s \leq s_m \quad (3-a)$$

where τ is the local bond stress, s the local slip, τ_m and s_m are bond stress and slip at the peak point, and α is a parameter that varies between 0 and 1. In the case of specimens with CFRP rods, the ascending branch is followed by a softening branch. This is well interpolated by an equation formally identical to (3-a):

$$\tau(s) = \tau_m \cdot \left(\frac{s}{s_m} \right)^{\alpha'} = C' \cdot s^{\alpha'} \quad s \geq s_m \quad (3-b)$$

in which α' varies between -1 and 0.

Parameters τ_m , s_m and α , calibrated by best fitting of the experimental results from the specimens with 4-diameter bonded length, are reported in Table 3. The average bond stress was plotted vs. the average value of loaded-end and free-end slips, and the resulting curve was used for calibration. Parameter α was obtained by equating the area underneath the ascending branch of the experimental curve to the value:

$$A_\tau(0, s_m) = \int_0^{s_m} \tau_m \left(\frac{s}{s_m} \right)^\alpha ds = \frac{\tau_m s_m}{1 + \alpha} \quad (4)$$

Another observation can be made on the τ -slip law for splitting failure. In a previous study, the local τ -slip law of specimens failed by splitting was obtained from strain data recorded along the bonded length [8] as consisting in one ascending branch according to (3), followed by a linear descending branch with a value of ultimate slip. The presence of such descending branch, due to the limited value of the ultimate slip, is very difficult to observe in specimens with short bonded lengths and can only be evidenced when deriving the local τ -slip relationship *indirectly*, that is, by means of load-slip curves of specimens with long bonded lengths as suggested in [14] or by means of strain data as shown in [8].

Bond Failure Load and Anchorage Length

Once the analytical τ – slip relationship is known, it can be used to analytically solve all problems related to the bond behavior, particularly, to calculate bond failure load and development length of NSM FRP rods. For a detailed explanation of the procedure, see [8].

When the bond – slip behavior of a joint is brittle (such as that of Figure 4-b), the bond failure load increases with the bonded length up to a certain value of bonded length, beyond which a further increase does not produce any benefit. In these cases, the maximum load sustainable by the joint is always lower than the ultimate strength of the bar and the development length, as traditionally intended, does not exist. This is, for instance, the case of NSM GFRP deformed rebars failing by splitting [8]. Conversely, for ductile bond – slip curves, the bond failure load indefinitely increases with the bonded length, until the tensile strength of the bar is reached for a value of bonded length that is the development length. This is the case of bond specimens with smooth groove surface failed at the epoxy – concrete interface [9], for which the bond – slip relationship is characterized by a first steep ascending branch followed by a descending branch approaching a constant value of bond stress. Hence, it may be demonstrated that, although the local bond strength is higher for specimens with rough grooves, the bond failure load of specimens with smooth grooves may be higher if the bonded length is long enough. This physically corresponds to the fact that, when the groove surface is smooth, local relative slip between epoxy and concrete relieves the stress state in the cover, thus delaying splitting and cracking.

From the design standpoint, the anchorage length of the rod has to be such that the free end does not slip under the design load, therefore, the load at onset of free-end slip has more practical interest of the bond failure load. Furthermore, it is often desired to anchor the rod using only the ascending portion of the τ – slip relationship. The maximum tensile stress that can be applied to the rod to satisfy this condition is [16]:

$$\sigma_1 = \sqrt{\frac{8 \cdot E_b \cdot \tau_m \cdot s_m}{d_b \cdot (1 + \alpha)}} \quad (8)$$

The corresponding minimum bonded length l_m can be expressed as:

$$l_m = \frac{\sigma_1 \cdot d_b \cdot (1 + \alpha)}{4 \cdot \tau_m} \quad (9)$$

The computed values of σ_1 and l_m are reported in Table 3. The low values of σ_1 / σ_u , σ_u being the ultimate tensile load of the FRP rods, indicate that bond is the controlling factor on design and limits the efficiency in the use of the FRP material.

Table 3. Calibrated Parameters in the τ – slip relationships and Values of σ_1 and l_m

Specimen Code	τ_m [MPa]	s_m [mm]	α	σ_1 [MPa]	σ_1 / σ_u [%]	l_m (n° of nominal d_b)
CR/a	11.24	0.203	0.80	341.5	17.0	68
CR/b	15.35	0.161	0.90	346.0	17.2	107
CR/c	16.56	0.878	0.92	834.8	41.4	30
GR/a	9.14	0.075	0.35	126.0	14.4	7
GR/c	12.48	0.177	0.56	211.0	24.1	15

Conclusions

A series of 12 specimens was tested to investigate the effect on the bond performance of bonded length, groove size, surface configuration of the rod and of the groove. Failure occurred in all cases by cracking of the concrete surrounding the groove upon formation and propagation of a longitudinal splitting crack in the epoxy cover. The average bond strength decreased as the bonded length increased, due to the non-uniform distribution of bond stresses, and increased with increasing groove size. The average bond strength of specimens with GFRP rebars was always lower than that of specimens with CFRP rebars and the same values of the remaining parameters. The reason was the higher relative rib area of GFRP, which produces a larger radial pressure for a given bond stress and thus anticipates failure and makes it more brittle. The ultimate load of some specimens was compared with that of identical specimens having smooth groove surface and failed at the epoxy – concrete interface. As expected, the specimens with rough grooves failed in all cases at higher values of local bond stress. However, their bond – slip behavior was more brittle. From a theoretical standpoint, this indicates that the bond failure load of specimens with smooth grooves may become higher for long bonded lengths.

The local bond-slip relationships was approximated with the average bond stress-slip curves of the specimens with short bonded length and modeled analytically. This allowed to compute quantities of interest from a design standpoint, namely, the load at onset of free-end slip corresponding to the ascending portion of the bond-slip curve, and the corresponding anchorage length. It appears that bond is the controlling factor on design of NSM FRP rods.

Further specimens are being tested with spirally-wound and sanded CFRP rebars and cement-filled grooves. The experimental database needs to be enlarged in order to better characterize the bond-slip behavior of NSM FRP rods and the influence on it of the significant variables. Analytical and numerical (finite element) modeling is also underway.

Acknowledgements

The authors wish to acknowledge MAC Italia S.p.A. for supplying the epoxy used in this experimental program and FICES S.p.A for casting the concrete specimens free of charge. This

investigation was supported by the Italian Ministry of Research (MURST) under program COFIN2000.

References

1. Emmons, P., Thomas, J., and Sabnis, G.M. "New Strengthening Technology Developed – Blue Circle Cement Silo Repair and Upgrade", Proceedings of the International Workshop on Structural Composites for Infrastructure Applications, Cairo, Egypt, May 28-30 2001, pp. 97-107.
2. Asplund, S.O. "Strengthening Bridge Slabs with Grouted Reinforcement", Journal of the American Concrete Institute, 1949, Vol. 20, No. 6, January, pp. 397-406.
3. Warren, G.E. *Waterfront Repair and Upgrade, Advanced Technology Demonstration Site No. 2: Pier 12, NAVSTA San Diego*, Site Specific Report SSR-2419-SHR, NFESC, 1998, Port Hueneme, CA.
4. Warren, G.E. *Waterfront Repair and Upgrade, Advanced Technology Demonstration Site No. 3: NAVSTA Bravo 25, Pearl Harbour*, Site Specific Report SSR-2567-SHR, NFESC, 2000, Port Hueneme, CA.
5. Yan, X.; Miller, B.; Nanni, A.; and Bakis, C.E. "Characterization of CFRP Bars Used as Near-Surface Mounted Reinforcement", Proc. 8th International Structural Faults and Repair Conference, M.C. Forde, Ed., Engineering Technics Press, Edinburgh, Scotland, 1999, 10 pp., CD-ROM version.
6. De Lorenzis, L., and Nanni, A. "Shear Strengthening of RC Beams with Near Surface Mounted FRP Rods," *ACI Structural Journal*, 2001, Vol. 98, No. 1.
7. De Lorenzis, L., and Nanni, A. "Characterization of FRP Rods as Near-Surface Mounted Reinforcement", *ASCE Journal of Composites for Construction*, 2001, Vol. 5, No. 2, pp. 114-121.
8. De Lorenzis, L., Nanni, A. "Bond of Near-Surface Mounted FRP Rods to Concrete", *ACI Structural Journal*, 2002, in press.
9. De Lorenzis, L., Rizzo, A., and La Tegola, A. "A Modified Pull-Out Test for Bond of Near-Surface Mounted FRP Reinforcement in Concrete", *Composites Part B: Engineering*, 2002, submitted for publication.
10. Tepfers, R. *A Theory of Bond Applied to Overlapped Tensile Reinforcement Splices for Deformed Bars*, Publication 73:2, Division of Concrete Structures, Chalmers University of Technology, Gothenburg, Sweden, 1973, 328 pp.
11. CEB. CEB-FIP Model Code 1990, CEB Bulletin d'Information No. 213/214, Lausanne 1993.
12. van der Veen, C., *Cryogenic Bond Stress – Slip Relationship*, Delft University of Technology, Doctoral Thesis, Delft, The Netherlands, 1990, 111 pp.
13. Rosati, G., and Schumm, C., "An Identification Procedure of Fracture Energy in Concrete: Mathematical Modeling and Experimental Verification", Proceedings of the RILEM/ESIS Conference on Fracture Process in Concrete, Rock and Ceramics, Noordwijk, The Netherlands, 1991, published by E. & F.N. Spon, London, 1991, Vol. 2, pp. 629-638.
14. Focacci, F.; Nanni, A.; and Bakis, C.E. "Local Bond-Slip Relationship for FRP Reinforcement in Concrete", *Journal of Composites for Construction*, 2000, Vol. 4, No. 1, pp. 1-9.
15. Eligehausen, R.; Popov, E. P.; and Bertero, V. V. "Local Bond Stress – Slip Relationships of Deformed Bars Under Generalized Excitations", Report No. 83/23, EERC, University of California, Berkeley, CA, 1983, 162 pp.
16. Cosenza, E.; Manfredi, G.; and Realfonzo, R. "Behavior and Modeling of Bond of FRP Rebars to Concrete", *Journal of Composites for Construction*, 1997, Vol. 1, No. 2, pp. 40-51.